Effects of Kraft lignin and corn cob agro-residue on the properties of injected-moulded biocomposites

Hélène de Baynast, Amélie Tribot, Benjamin Niez, Fabrice Audonnet, Eric Badel, Guy Cesar, Claude-Gilles Dussap, Emmanuelle Gastaldi, Laurent Massacrier, Philippe Michaud, et al.

Effects of Kraft Lignin and Corn Cob agro-residue on the properties of injected-moulded Biocompo-sites

Hélène de Baynast[1], Amélie Tribot[1], Benjamin Niez[2], Fabrice Audonnet[1], Eric Badel[2], Guy Cesar[3], Claude-Gilles Dussap[2], Emmanuelle Gastaldi[4], Laurent Massacrier[5], Philippe Michaud[1,*] and Cédric Delattre[1,6]

[1] Université Clermont Auvergne, Clermont Auvergne INP, CNRS, Institut Pascal, F-63000 Clermont-Ferrand, France; amelie.tribot@uca.fr (A.T.); fabrice.audonnet@uca.fr (F.A.); helene.de-baynast@uca.fr (H.de.B.); cedric.delattre@uca.fr (C.D.); philippe.michaud@uca.fr (P.M)

[2] Université Clermont Auvergne, INRAE, PIAF, F-63000 Clermont-Ferrand, France; eric.badel@uca.fr (E.B.); benjamin.niez@uca.fr (B.N.)

[3] POLYBIOAID - SERPBIO, Compositic-Université Bretagne Sud, F-56321, Lorient, France

[4] UMR IATE Univ. Montpellier/INRAE/Montpellier Supagro, F-34060 Montpellier, France; emmanu-elle.gastaldi@umontpellier.fr

[5] Green & Business Consulting Company, F-63000 Clermont-Ferrand, France; lau-rent.massacrier@gbcc.bio

[6] Institut Universitaire de France (IUF), 1 Rue Descartes, 75005 Paris, France; cedric.delattre@uca.fr

* Correspondence: philippe.michaud@uca.fr; Tel.: +33473407425

Abstract: Lignocellulosic by-products are frequently disposed by means of combustion. This study investigates an alternative route for corn cob and Kraft lignin resources in order to support circular economy. The respective plant-based fibres and filler were compounded for the first time together with a poly(lactic acid) (PLA) matrix. Consecutively, seven different biocomposites were processed by injection-moulding and further characterized. The biocomposite containing a mixture of Kraft lignin and corn cob (12 wt% in total) exhibited the highest flexural strength (84 MPa). A proper wetting of PLA onto the corn cob particles demonstrated a good compatibility at matrix/fibre interface. PLA molecular structure changed in presence of 20 wt% lignin filler, with effect on the glass transition temperature and on the composite mechanical strength. The fibres moderately influenced composites surface tension, while Kraft lignin contributed to a slight increase of surface hydrophobicity. Surface energy (σsTotal) of composites have been estimated at 27.6, 28.7 and 27.8 mN/m for PLA/KL-20, PLA/CC-10 and PLA/KL-15/CC-5 respectively. While the polar component (σsPolar) have been estimated at 17.8, 20.0 and 18.7 mN/m for

PLA/KL-20, PLA/CC-10 and PLA/KL-15/CC-5 respectively. Unlike the PLA/corn cob composite, those containing Kraft lignin were entirely biodegraded within 2 months in industrial composting conditions study. The materials could be utilised for end-use products thanks to their good mechanical and thermal properties. By adding wood-lignin and corn by-products, materials cost and carbon footprint shall decrease in comparison to pure PLA, while being a biodegradable and sustainable replacement of polyolefins.

Keywords: Natural fibers; Biopolymer; Environmental degradation; Mechanical properties; Thermal analysis; Microstructure

1. Introduction

Poly(lactic acid) (PLA) is one of the most extensively studied biopolymers. Nowadays, it has found its way onto the plastic market to deliver sustainable products to customers (Skoczinski et al., 2021). PLA is bio-based and rapidly biodegradable in industrial compost (Gorrasi and Pantani, 2013; Musioł et al., 2016), having the potential to address global challenges such as depletion of fossil resources and microplastics-induced pollution of lands (Sin and Tueen, 2019). For improved sustainability (durability, degradability) and performance (thermal, crystallisation, mechanical properties), multitude of authors have investigated the addition of lignocellulosic fibres, particles or agricultural wastes in PLA-based composites (Mansor et al., 2015; Misra et al., 2015; Rajeshkumar et al., 2021; Siakeng et al., 2019).

The novelty of this study is the concomitant use of one wood-based filler and one agricultural by-product, namely Kraft lignin and corn cob, to reinforce the PLA. Kraft lignin (KL) is a widely available by-product from wood Kraft pulping industry. After securing pulp mill in energy, KL global production has been estimated to 75,000 tonnes per year (Miller et al., 2016), and its production capacity to 265,000 tonnes per year (Dessbesell et al., 2020). Corn cob (CC) is a lignocellulosic by-product from crops industry which needs to be crushed for its utilisation into composites. CC is mainly composed of 35-46 wt% glucan (cellulose), 28-42 wt% xylan (hemicellulose), and 11-18 wt% lignin (Guo et al., 2014; Kumar et al., 2010; Li et al., 2014; Schwietzke et al., 2009). ~~It was supposed that KL and CC can synergically improve mechanical properties of PLA-based composites~~. Filling PLA with lignocellulosic by-products seemed to be an economical solution as bioplastics not yet compete the prices of the fossil-based counter-

parts such as polyethylene (PE) and polyethylene terephthalate (PET) (Skoczinski et al., 2021). Nanopowders were known to nucleate polymer crystallisation, decreases its cold crystallisation temperature that led to an increase of modulus of elasticity and a decrease of the elongation at break (Lezak et al. 2008). The addition of long natural fibres is known to increase tensile and flexural strength (Ravi Theja Reddy et al. 2021). For example, Agustin-Salazar et al. showed that lignin and agricultural by-product (pecan nutshell) separately improved the mechanical properties of PLA-based composites but they didn't mixed the fillers (Agustin-Salazar et al., 2018). It was supposed that KL and CC can synergistically have a beneficial effect.

The purpose of the work was to validate the concept of KL-CC-PLA ternary system with exploratory formulations and overcome the loss in different PLA properties when only KL or CC were used. Few studies have presented the biodegradation kinetic of PLA biocomposites in industrial composting conditions. Specifically, there was a research gap concerning the biodegradation of PLA-lignin composites. It is known that not many microorganisms have the ability to degrade native lignin (mainly white-rot fungi) (Nilsson, 2009). Therefore, a relatively slow biodegradation rate was expected for KL-rich formulations compared to CC-rich formulation containing cellulose.

Technical lignins confer attractive properties to polymers, including fire-resistivity, UV-stability, and mechanical stiffness (Berlin and Balakshin, 2014; Faruk and Sain, 2015; Mimini et al., 2019; Poletto, 2018; Spiridon et al., 2015). However, a decrease in mechanical strength has been systematically reported when 5 wt% to maximum 20 wt% of lignin filler was incorporated into PLA (Anwer et al., 2015; Gkartzou et al., 2017; Gordobil et al., 2015; Kumar et al., 2019; Mimini et al., 2019; Spiridon et al., 2015; Tanase-Opedal et al., 2019). To minimize the loss of mechanical strength and to improve PLA-lignin miscibility, silane coupling agent has been used (Wang et al. 2020). E-beam irradiation of lignin has been previously conducted (Kumar et al., 2019), or acetylated lignin has been used (Gordobil et al., 2014). The latest also seemed to prevent hydrolytic degradation of PLA. Some authors reported increased thermal stability (Gordobil et al., 2015; Spiridon et al., 2015) and hydrophobicity (Gordobil et al., 2015, 2014; Spiridon et al., 2015) by addition of Kraft lignin to PLA. Bužarovska et al. (2021) have demonstrated the good biocompatibility and very low cytotoxicity of PLA/lignin films and measured increased photodegradation and improved water barrier properties up to 73% compared to pure PLA.

Few PLA/CC composites were studied earlier, and they were prepared by compression moulding methods. Chun et al. (2014) analysed mechanical, thermal, and morphological properties of PLA eco-composites containing 10 to 40 wt% CC powder and coconut oil-based coupling agent. Faludi et al. (2013) studied PLA biocomposites filled with 5 to 60 wt% CC particles in terms of tensile properties and microstructure. The reader may also refer to a previous study where we have developed bio-based composites reinforced with same CC particles using compression moulding method without heating in a lignosulfonates matrix (Tribot et al., 2018). The injection-moulding technique has been employed to process CC filled biocomposites with high-density polyethylene (HDPE) (Ogah and Afiukwa, 2014) or polypropylene (PP) matrices (Onuoha et al., 2017; Wan et al., 2018), but to our knowledge not with PLA. Lignocellulosic material, such as CC, frequently lightweight the thermoplastic matrices and sometimes boost their mechanical properties (Mansor et al., 2015; Misra et al., 2015). In general, composites filled with natural fibres are eco-friendly materials but some challenges remain. One of the biggest issue is water absorption of the fibres due to their hydrophilic nature, causing dimensional variations of the matrix, formation of micro-cracks and weaker mechanical resistance (Azwa et al., 2013; Stark and Gardner, 2008).

This paper presents seven PLA-based materials filled with KL and/or CC particles. The novel compositions have been processed using conventional techniques, namely twin-screw extrusion and injection-moulding. The developed materials were extensively characterized thanks to mechanical tests, thermal analyses (DSC and TGA), scanning electron microscopy (SEM), surface energy analyses, Fourier-transformed infrared spectroscopy (FT-IR), and respirometric tests to assess their biodegradability in industrial composting conditions.

2. Materials and Methods

2.1. Raw materials

PLA Ingeo™ from NatureWorks (grade 4043D) was utilised in pellet form. Kraft lignin (KL) was provided by FPInnovations (LignoForce™ Canadian production system). KL average particle size (D50) was 47 µm and carbon content ((62.28±0.16) wt%) using elementary analysis. Dried corn cob (CC) originated from Limagrain production in Ennezat, France (intermediate flint-dent CC variety) is composed of ash (1.4-2 wt%), Klason lignin ((11.17±0.16) wt%) and carbon ((43.58±0.29) wt%).

2.2. Composites fabrication 111

Firstly, lignocellulosic particles were prepared by crushing the CC (**Figure 1a**). Secondly, PLA with 112
KL and/or CC were melt-compounded in order to improve dispersion of the particles inside PLA matrix. 113
Finally, test samples (**Figure 1b**) were prepared by injection moulding. 114

Figure 1 should be inserted here. 115

2.2.1. Corn cobs crushing 116

The CC crushing operated with cutting mill SM300 from Retsch at 1500rpm speed cut (**Figure 1a**). 117
Consequently, Control-lab sieve-tronic equipment accomplished particles sieving. To preserve resulting 118
sieved batches from moisture absorption, the particles remained in sealed containers at room temperature 119
until compounding. The CC particles that were not retained by a 400 µm mesh were discarded to avoid 120
the aggregation of the smallest fibres during extrusion (Ogah and Afiukwa, 2014). Were also discarded 121
the biggest CC particles that were not retained by a 800µm mesh, to be able to inject CC in the mould. 122
According data from our previous study (Tribot et al., 2018), the selected CC particles were assumed to 123
be wider than 240 µm. They had non-circular shapes with aspect ratio parameter (particle width divided 124
by its length) of (0.65±0.15). They also presented a rough surface with a convex parameter, defined as the 125
ratio between the convex hull perimeter and the actual perimeter of the particle, of (0.8±0.1) µm. 126

2.2.2. Compounding 127

Biopolymers and CC particles were blended at Valagro Carbone Renouvelable (Poitiers, France) by 128
means of co-rotating CLEXTRAL BC 21 twin-screw extruder (25 mm screw diameter and L:D ratio of 129
24). The recipes contained PLA, KL and/or CC are presented in the **Table 1**. 130

Table 1 should be inserted here. 131

During extrusion, a vacuum pump dispensed 40 mbar pressure for gas removal. A room-temperature 132
water bath completed cool down of the extruded strands prior pelletization. 133

2.2.3. Injection moulding 134

Billion H280/90 injection moulding equipment (control version Visumat 5005 SV) enabled to manu- 135
facture seven composites' formulations (**Table 2**). 136

Table 2 should be inserted here. 137

The material granulates were dried over night at 60°C before injection moulding. The injection cycle started with the hydraulically powered clamping unit securely closing the mould with a 900 kN force. The mould remained at room temperature during processing. Inside the barrel, the 38mm diameter reciprocating screw moved the material forward at a rotating speed of 200 rpm. Four heaters enabled progressive melting up to 105-170°C, optimized depending on the material composition. The hydraulic injection pressure reached (11±1) MPa. The molten material exited nozzle at 10.8 mm s^{-1} injection rate and experienced compaction at 3.6 mm s^{-1} rate. The mould design allowed to prepare four test specimens per cycle. After 15 seconds cooling, pins ejected the solidified sample out of the mould cavity with a 31 kN force. Prior to plastic injection, silicon release agent was sprayed onto mould cavity surfaces to facilitate ejection. The final specimens (**Figure 1b**) sized 122 x 10 x 4 mm for an average weight of 6 g, *i.e.*, a density of 1230 kg m^{-3}. They were placed seven days in a control room chamber prior to analysis.

2.3. Mechanical tests

2.3.1. Flexural tests

An Instron testing system 5565, equipped with a 1 kN force cell and piloted by Bluehill testing software, permitted the evaluation of flexural properties through three-points bending tests, according to the standard method ISO 178:2011. The span between specimens supports equalled 90 mm. The specimens were submitted to a load in the centre of the rectangular beam. The displacement speed of this central crosshead was 5 mm min^{-1}. Analyses started with three consecutive loading-unloading static cycles in the elastic zone of the materials. Then, materials experienced a final loading step until failure. The testing system continuously recorded displacement and force data. A number of 10 samples was tested for each recipe. Room conditions were 27°C and 30% relative humidity. Analyses of the experimental curves were performed using Matlab® software and specific programs. From the strain-stress curves we extracted the maximum stress, the maximum flexural strain, and the flexural elastic modulus of the beam. The flexural modulus of elasticity indicated the stiffness of the materials.

2.3.2. Vickers Hardness (HV)

Vickers hardness (HV) analyses were performed using a Mitutoyo MVK-H0 hardness tester. Applied load was 100 g force on the composite PLA/KL-20 and 50 g force on PLA and composites

PLA/CC-10, PLA/KL-10, and PLA/KL-15/CC-15, during 15 s. HV tests relied on operator measurement using a digital ocular at x100 magnification. Average values of hardness resulted from thirty-five tests point for each material formulation.

2.4. Thermal analyses

2.4.1. Thermogravimetric Analysis (TGA)

TGA measurements involved a TGA 2050 thermogravimetric analyser. Software for data recording and analysis were respectively TA Instrument Control and Universal Analysis 2000. Biocomposites samples were cut into 28 – 30 mg parts and put in the heat chamber. TGA proceeded with heating ramp of 10°C min^{-1} from room temperature to 900°C under 80 mL·min^{-1} nitrogen flow. Characteristic parameters such as ONSET temperature (T_{ONSET}), OFFSET temperature (T_{OFFSET}), and residual weight were recorded. They correspond to the point of intersection of the starting-mass baseline (T_{ONSET}) or final-mass baseline (T_{OFFSET}) and the tangent to the TGA curve at the point of maximum gradient. Differential thermogravimetric signal (DTG) was plotted in function of temperature and its extremum denoted MIDSET degradation temperature.

2.4.2. Differential Scanning Calorimetry (DSC)

Thermal events of PLA such as glass transition (Tg), melting (Tm) and cold crystallization (Tcc) were highlighted by means of differential scanning calorimeter Q2000 from TA Instruments. Data recording and analysis employed respectively TA Instrument Explorer and TA Universal Analysis software. Heat/Cool/Heat cycles were performed under nitrogen atmosphere (N_2, 25 mL min^{-1}) on 10 mg composite samples, including consecutively -50°C isotherm for 2 minutes, 10°C min^{-1} heating ramp from -50 to 200°C, 200°C isotherm for 2 minutes, and 10°C min^{-1} cooling ramp from 200°C to -50°C. The Tg of PLA was determined from data of the second cooling. Only the fraction weight of PLA was used in the expression of the cold crystallisation and melting enthalpies, *i.e.* ΔHcc and ΔHm. The percentage of crystallinity was calculated according to Equation (1).

$$Xc\ (\%) = (\Delta Hm - \Delta Hcc) \times 100 / \Delta Hm \qquad (1)$$

To evaluate the Tg of KL, we employed modulated DSC (MDSC) technique with a signal of 60 seconds period and ±0.8°C amplitude.

2.5. Fourier-Transformed Infrared Spectroscopy (FT-IR)

Test samples were analysed in the 400-4000 cm^{-1} spectral region with Brüker VERTEX 70 FT-IR spectrophotometer in attenuated total reflection mode (ATR diamond A225), completing 32 scans at 10 cm^{-1} resolution.

2.6. Scanning Electron Microscopy (SEM)

A JEOL 5910 LV Scanning Electron Microscope was used to observe the surface of failed specimens using a backscattering electron detector. Gold metallization was performed for 2 min with a current of 40 mA. The working distance and acceleration potential were equal to 19 mm and 5 kV respectively. Spirit software was used to the image acquisition.

2.7. Surface energy

Dispersive (σ_S^D) and polar (σ_S^P) fractions of material surface energy were evaluated according the Owens-Wendt method (Owens and Wendt, 1969). Four liquids allowed referencing, namely water, ethylene glycol, glycerol, and formamide. After the 5µl solvent droplet got stabilized on composites surface for 2 seconds, image acquisition was performed with camera Canon EOS 70D (W), sensor CMOS APS-C (20.2 megapixels) and lens Macro 150 mm F2,8 EX DG APO OS HSM. Contact angle measurements was evaluated by image analysis using Image J software. Materials received thirty different test points for each solvent reference.

2.8. Biodegradation in industrial compost

Biodegradation kinetic of milled biocomposites, KL filler, and CC filler was evaluated in composting conditions according to modified NF ISO 14855 standard. Carbon content of milled materials was measured with Flash 2000 Elemental Analyzer from Thermo Fischer Scientific at 1800°C. Standards dur-

ing elemental analysis were BBOT (2,5-bis(5-tert-butyl-benzoxazol-2-yl)thiophene) and ascorbic acid. Respirometric analyses utilized a mature green compost from waste management centre of Aspiran (France) which was sieved through 5 mm meshes. Biodegradation tests were conducted into 1L cylindrical hermetic glass vessels, each of them containing three 60mL opened flasks made of polypropylene. The first flask contained 6g of wet compost with a final water content of 50%, pH 8.05, and C/N ratio of 26.6 mixed together with 50mg carbon equivalent of each materials. The second flask contained 30 mL NaOH solution (0.1 mol L^{-1}) to trap the CO_2 produced by microorganisms. The third flask contained distilled water for keeping 100% relative humidity inside the vessel. Blank control consisted of compost only, while positive control consisted of microcellulose powder. Samples were allowed to incubate in the dark at (58±1)°C during 136 days. Incubation of KL was extended up to 317 days. At selected time interval, NaOH flasks were removed from the vessel for titration and then replaced by new NaOH solution containing flasks. Meanwhile, compost humidity was maintained constant by distilled water addition. Ultimate biodegradation (or mineralization) (Chevillard et al., 2011) was determined as the ratio of CO_2 released during material mineralization to the maximum CO_2 amount theoretically released by the material using Equation (2).

$$\text{Mineralization}(\%) = (m_{CO2\ test} - m_{CO2\ blank})/m_{CO2\ theoretical} \qquad (2)$$

where, $m_{CO2\ test}$ describes the CO_2 amount (mg) released by both compost medium respiration and material mineralization, $m_{CO2\ blank}$ is the CO_2 amount (mg) released by compost medium respiration, and $m_{CO2\ theoretical}$ is the maximal theoretical CO_2 amount (mg) released by material mineralization (calculated from elemental carbon content). Experimental biodegradation sigmoidal curves were modelled using Hill Equation (Equation (3)) (Calmon et al., 2000; Décriaud-Calmon, 1998).

$$Deg(t) = (Deg_{max} \times t^n)/(k^n + t^n) \qquad (3)$$

where Deg at time t (day) is the percentage degradation, Deg_{max} is the percentage degradation at infinite time, k (day) is the time when Deg = 0.5 Deg_{max}.

The biodegradation curve of CC filler had a double sigmoid shape and was modelled according Boltzmann Equation (4).

$$Deg(t) = Deg_1+(Deg_2-Deg_1)\times\{p/(1+10^{h1\,(k1-t)})+(1-p)/(1+10^{h2\,(k2-t)})\} \qquad (4)$$

where Deg_1 at time t_1 (day) the maximum percentage degradation of the first sigmoid, Deg_2 at time t_2 (day) is the maximum percentage degradation of the second sigmoid, p is the proportion of the first sigmoid to the total curve, h_1 and h_2 are respectively the slopes of first and second sigmoids, k_1 (day) is the time when Deg = 0.5 Deg_1, and k_2 (day) is the time when Deg = 0.5 Deg_2.

3. Results

3.1. Fourier-transformed infrared spectroscopy (FT-IR)

CC macro- and microstructure was heterogeneous with a porous and light pith in the centre surrounded by strong woody ring and chaff (Faludi et al., 2013). Despite their different physical properties, the three parts of CC exhibited close chemical identity (**Figure 2a**).

Figure 2 should be inserted here.

The vibration at 1726 cm^{-1} was assigned to C=O stretching of hemicellulose. The 3340 cm^{-1} band, corresponding to OH stretching of intra- and inter- molecular hydrogen bonds was particularly intense in pith FT-IR spectrum. Similarly, vibration band at 1036 cm^{-1}, attributed to C-O stretching of polysaccharides ester and ether groups was very intense in the pith. Thus, the central part of corn cob seemed to be more hydrophilic than woody ring and chaff. The woody ring contained a higher proportion of lignin since vibration bands at 2920 and 2853 cm^{-1} are typical of lignin CH stretching in methyl and methylene groups (**Figure 2c**). The composites presented a similar pattern that their PLA matrix. The characteristic vibration band at 1750 cm^{-1} corresponded to C=O stretching in PLA ester carbonyl group (**Figure 2b, d-f**). Vibration of hydroxyl groups around 3300 cm^{-1} was not systematically reported in composites. However, in pure PLA the OH carboxylic acid or alcohol terminal groups were evidenced at 3299 cm^{-1} (**Figure 2b**) (Kumar et al., 2019). The vibration band at 1182 cm^{-1} was arising from PLA ester C-O-C asymmetric stretching. Its intensity particularly decreased for sample PLA/KL-20 (**Figure 2d**), thus polymer chain scission is likely to occur at the C-O bond in presence of Kraft lignin (Kumar et al., 2019). This assumption was comforted by the lower intensity of 1128 cm^{-1} shoulder peak in presence of 20 %wt KL. Hypothetically, extrusion process could also have favoured PLA-lignin covalent coupling. Mimini et al.

(2019) have studied non-catalysed esterification between COOH terminal groups of PLA and OH (phenolic or aliphatic) groups of unmodified lignin by ^{31}P NMR analytical method. Symmetric and asymmetric C-H stretching of PLA CH_3 groups were visible at 2997 cm^{-1}, 2921 cm^{-1}, and 2852 cm^{-1} (**Figure 2b**). A new vibration band appeared at 2961 cm^{-1} in samples containing KL, assigned to CH stretching in methyl and methylene groups of lignin side chains (**Figure 2d**). Vibration bands at 1596 cm^{-1} and 1513 cm^{-1} were associated with conjugated carbonyl/carboxyl C=C skeletal vibrations of Kraft lignin in PLA/KL-20 and PLA/KL-10 spectra (Gordobil et al., 2014). Vibration bands at 1453 cm^{-1}, 955 cm^{-1}, 870 cm^{-1}, and 755 cm^{-1} corresponded respectively to methyl/methylene deformation, C-CH_3 stretching, -C-C- stretching amorphous, and -C-C- stretching crystalline phases of PLA. The intensity of the 1260 cm^{-1} band increased with 20wt% KL due to G ring breathing of lignin (**Figure 2d**) (Gordobil et al., 2014). The 921 cm^{-1} vibration band could be assigned to the –C–OH bending of the carboxylic acid groups in PLA. Finally, the absorption band at 800 cm^{-1} was assigned to CH deformation of KL aromatic ring. As well-known, the vibrations of C=C bonds of the aromatic rings are visible at around 1596 and 1513 cm^{-1}. As a general rule, when the aromatic rings of lignin are not fully substituted, we can observed the presence of aromatic H visible at around 800 cm^{-1} (Gordobil et al., 2014). We suggested that the disappearance of this peak on the other spectra can be interpreted as a complete substitution of aromatic groups.

3.2. Thermal properties (TGA and DSC)

Thermal resistance of raw materials (CC, KL, PLA) and composites was evaluated by TGA (**Figure 3**). CC particles and KL powder tended to absorb moisture and bond water molecules.

Figure 3 should be inserted here.

Upon heating, 6 wt% of free water evaporated between 20 and 141°C for CC and at 58°C for KL sample. TGA and DTG curves (**Figure 3b**) of CC were close to those presented by Panthapulakkal and Sain (2007). The authors assessed thermal stability of CC up to 200°C, encouraging its use to replace wood fibres in thermoplastic composites. In the same way, CC was thermally stable at 200°C with ONSET temperature of 297°C and two main degradation peaks at 334 and 363°C. When degradation of CC was completed, residual weight of the sample equalled 19.8 wt% of its initial mass (**Figure 3a**). The ON-

SET temperature of 314°C demonstrated that KL was slightly more thermo-resistant than CC. Condensed chemical structures of lignin led to relatively high residual weights, such as 40 wt% in this study. A higher content of KL implied a higher residual weight of composites subjected to thermal degradation (**Figure 3a**) as established in earlier studies on PLA-lignin material (Gordobil et al., 2015; Mimini et al., 2019; Tanase-Opedal et al., 2019).

KL decomposed according to a complex pathway until it reached 484°C OFFSET temperature. It was also noted that degradation was more temperature-dispersed for KL than for PLA (**Figure 3b**). Therefore, when all the polyester phase of composite is consumed, degradation of lignin aromatics would still be ongoing. CC or KL filler decreased materials thermal stability in comparison to pure PLA, with evidence of 13 to 55°C lower degradation temperatures. This finding corroborates Tg results of Tanase-Opedal et al. (2019) in presence of 20 wt% Soda lignin. However, some authors claimed that thermal stability of material got improved by addition of less than 10 wt% Kraft lignin to PLA (Gordobil et al., 2015; Spiridon et al., 2015). Variability of lignin structure and molecular weights might explain these distinct influences on PLA thermal stability. Lignocellulosic fibres are frequently less stable than polymer matrices (Goriparthi et al., 2012; Siakeng et al., 2019; Wang et al., 2018). Accordingly, CC filler did not enhance thermal stability of PLA.

The DSC curves are presented in **Figure 3c**. The effects of CC particles and KL filler on the glass transition, the crystallisation and the melting thermal events of PLA were evaluated. The glass transition of KL could be measured by MDSC and valued 86°C. A higher Tg would have been expected for a condensed lignin but same value has been previously reported in the literature for a softwood Kraft lignin (Gordobil et al., 2016). Tg of PLA slightly decreased relatively to filler content (**Table 3**).

Table 3 should be inserted here.

Glass transition is associated with the mobility of polymer' chains and depends also on the molecular weight. This suggested that CC and KL could favour chain mobility of PLA by preventing hydrogen bonding between polyester functional groups. Most important modifications of Tg were for composite containing {15 %wt KL + 5 % wt CC} and 20 wt% KL, dropping from 60.5 to 55.9°C and to 56.4°C respectively (**Table 3**). This confirms the scission of PLA' chains observed with FT-IR analyses. This effect of lignin on PLA glass transition is aligned with finding of prior studies (Kumar et al., 2019; Mimini

et al., 2019; Spiridon et al., 2015). We hypothetically think that KL has re-hydrated before compounding, and that the residual water was responsible for PLA hydrolysis. The PLA oligomers (low molecular weights) formed had the potential to auto-plasticize PLA, therefore decreasing its Tg. Then, the cold crystallisation (Mimini et al., 2019) event was identified through the exothermic signal at 117 - 125°C (**Table 3**). Above its Tg, PLA polymer chains gained mobility, thus they were able to order to form crystal phases. Melting of crystallites occurred at 147 - 152°C (**Table 3**) as emphasized by the endothermic signal. No crystallisation event happened during cool down of the samples. With increased filler content, both ΔHm and ~~ΔHc~~ ΔHcc exhibited up to 5-6 times fold increase (**Table 3**), except for adding KL alone. This result suggested that CC acted as nucleating agents and were able to favour crystallisation of PLA chains. The analysis of CC particles shape parameters (Tribot et al., 2018) demonstrated their rough surface, which supports a nucleation ability. At given 10°C min^{-1} heating rate, as the filler content increased, the presence of a double melting peak was also accentuated (**Figure 3c**). This result means that two distinct lamellae populations had formed during cold crystallization. This was analysed in several studies dealing with lignocellulosic fibres (Komal et al., 2020; Kumar and Tumu, 2019; Lila et al., 2019; Tan et al., 2019) or technical lignins (Gkartzou et al., 2017; Mimini et al., 2019; Tanase-Opedal et al., 2019) in PLA, most frequently by XRD. However, it is noted that addition of KL alone has a negative effect on the crystallisation. This is in accordance with Gordobil et al. (2014) who found that the presence of lignin filler disfavoured lamellae formation.

~~3.4~~3.3. Composites microstructure

Fracture surfaces of flexion-loaded specimens were inspected by scanning electron microscopy (SEM) (**Figure ~~5~~4**).

Figure ~~5~~4 should be inserted here.

PLA presented a brittle fracture pattern (**Figure 4a**). Composite containing 10 wt% of KL revealed a rough fractured surface (**Figure 4b**). Locally, even more pronounced roughness was observed for 20 wt% KL (**Figure 4c**). Gao and Qiang (2017) reported a correlation between cellulose particle size to fracture pattern in PLA-based composites. In their work, the authors detected a rougher surface and consequently higher fractal dimension when the cellulose particles were the smallest (39 µm). Our KL particles of me-

dian size of 47 µm seemed to generate a similar effect. PLA/KL composites would be able to absorb higher work of fracture as indicated by improved hardness and stiffness of these materials. SEM allowed inspection of CC particles and polymer-CC interface. Fractured surface was more irregular as CC content increased (**Figure 4g**). Unbounding of some CC particles could be noticed (**Figure 4f,h**). Nevertheless, PLA-CC adhesion was good as assessed by proper wetting of the matrix on CC surface (**Figure 4d,f**). Among tested composites, the ones with better flexural strength (PLA/KL-2.5/CC-9) had no major fibre de-bonding (**Figure 4e**). The fractography of these composites shown more ductile zones than for the others.

3.~~3~~4. Flexural and hardness properties

Mechanical properties of the composites were evaluated by means of hardness (**Figure 45a**) and flexural tests (**Figure 5**).

Figure 5 should be inserted here.

Positive effect of KL filler on materials hardness was measured. The composite PLA/KL-20 exhibited the highest hardness (25.6±3.4) HV. These values are coherent with results of 18 – 20 HV found by Spiridon et al. (2015) for PLA/Kraft lignin-filled composites (max 15 wt% filler). In our study, hardness increased by 17% and 47% with respectively 10 wt% and 20 wt% KL loading into PLA (**Figure 5a**). This tendency aligned with the stiffness results since composites flexural modulus increased by 17% with 20% KL addition to PLA matrix (**Figure 5b**). However, CC addition did not impact the average hardness of PLA. The composites structural inhomogeneity explained the wide standard deviation of hardness values. For instance, CC pith particles were softer and CC woody particles were harder than PLA matrix. Nevertheless, upon addition of 5 wt% CC mixed with 15 wt% KL (sample PLA/KL-15/CC-5), average hardness increased by 13% compared to pure PLA. Both technical lignins and lignocellulosic particles are prone to enhance stiffness as shown for PLA/corn fibres (Luo et al., 2014) or PLA/lignin (Gordobil et al., 2015; Kumar et al., 2019; Mimini et al., 2019) composites.

All composites tested exhibited higher stiffness than PLA, showing the positive effect of CC and KL filler on this mechanical property (**Figure 5b**). At the highest fibre content (sample PLA/KL-2.5/CC-19), flexural modulus equalled (3.7±0.1) GPa (20% increase compared to pure PLA). On the contrary, materi-

als flexural strength was negatively impacted by KL or CC filler. The debonding of some CC particles observed with SEM can partially explained this loss of flexural strength. Higher KL content was especially responsible for mechanical strength loss (**Figure 5b**). This result is in accordance with prior investigations on PLA/lignin (Gkartzou et al., 2017; Gordobil et al., 2015; Kumar et al., 2019; Mimini et al., 2019; Spiridon et al., 2015; Tanase-Opedal et al., 2019). Composite PLA/KL-20 exhibited the lowest flexural strength (56.4±4.2) MPa, meaning 38% less strength than PLA. The addition of KL has had the effect of reducing the plastic zone of composites. For PLA/KL-10 the rupture took place as it left the elastic zone, with a maximal flexural strain of 1.6% while the value was 4.1% for PLA alone, confirming the fragile aspect of the fracture facies. Different causes may explain this result. In one hand, FT-IR analysis revealed hydrolysis of PLA ether groups and/or potential PLA-lignin covalent bonding. Thus, such modifications on the polymer chains may have weakened the mechanical strength of the matrix. The effect of this chains' modification has reduced the effect of the chains mobility observed by DSC and FT-IR analyses. In other hand, KL acted as a rigid filler that initiated cracking of the PLA matrix as evidenced by SEM. Surprisingly, composite PLA/KL-2.5/CC-9 exhibited a flexural strength of (83.7±0.7) MPa which is only 8% less than PLA. Therefore, synergetic effects of KL and CC mixing may impact positively mechanical properties of the biocomposites.

3.5. Surface energy

Surface energy of PLA and composites with 20 wt% KL, 10 wt% CC, and 15 wt% KL plus 5 wt% CC were calculated thanks to contact angle measurement of solvent drops (**Table 4**).

Table 4 should be inserted here.

Contact angle of water (θ_{water}) was less than 90°, thus PLA and composites showed a hydrophilic surface. Native lignin is known to provide hydrophobicity to wood cells. Some technical lignin counterparts are known to show similar behaviour in polymer composites (Gao and Qiang, 2017; Gordobil et al., 2015, 2014; Spiridon et al., 2015). Presently, water was found to wet the PLA/KL-20 surface less than the PLA surface with respective θ_{water} of 80.5 and 73.2°. Also, the σ_s^{Polar}/ $\sigma_s^{Dispersive}$ ratio dropped from 2.0 for PLA to 1.8 for composite PLA/KL-20, assessing the hydrophobic capacity of KL. CC particles also impacted

the surface energy of composites, since the $\sigma_s^{Polar}/\sigma_s^{Dispersive}$ ratio increased from 2.0 to 2.3 by addition of 10 wt% CC compared to pure PLA.

3.6. Biodegradability in industrial compost

The biodegradability of PLA composites was assessed through the general method of measurement of CO_2 released under composting conditions at 58°C (**Table 5**).

Table 5 should be inserted here.

According to ISO norm, the respirometric tests were assumed to be valided since the cellulose control sample exceeded 70% biodegradation after 21 days (NF ISO 14855). Such as cellulose, CC was 100% biodegraded at day 120, showing an easy decomposition of CC material in the compost medium. Its degradation kinetic was somewhat different than observed for cellulose as standard (**Figure 6a**).

Figure 6 should be inserted here.

In contrast to cellulose, CC biodegradation occurred in a two-steps mechanism. This was modelled with a double sigmoid representation according to Boltzmann Equation (**Table 5b**). The slope of the first sigmoid equalled 0.330, against 0.036 for the second sigmoid slope. Thus, the first degradation step was 10 times faster than the second one. This result would mean that different microorganisms were involved. We can suggest that one microorganisms population could contribute to the primary fast CC biodegradation rate (half time of 3 days) whereas a second microorganisms population would slowly degrade its remaining products (half time of 43 days) up to 100% biodegradation. As a general rule, it is well-known that natural lignin can be mineralized in composting conditions by some microfungi, excluding the white-rot fungi which do not survive the thermophilic composting phase (Tuomela et al., 2000). On the contrary, Kraft lignins own a carbon structure more condensed than natural lignin, which can be an obstacle to microbial actions (David et al., 2019). Although the duration of KL mineralization test was extended up to 317 days, the lignin filler was the last degraded compound in our study (Deg_{max} of 64%). Few studies have investigated the effect of lignin fillers on composites biodegradation rate. In their research, Da Silva et al. (2019) weighted residual mass of PLA and PLA/lignin composites after 180 days burial in soil compost. Their results showed that PLA/lignin composites were not easily degraded in soil medium with maximum 5% mass loss. Composite with 15% lignin content was less degraded than the ones containing

5 or 10% lignin. PLA has a glass transition temperature around 50-60°C, therefore it is known that the industrial composting conditions are the most suitable to ensure its fast decomposition. In our study, with compost temperature over PLA glass transition, PLA composites containing KL reached total degradation within 63 days. Therefore, KL could be fully degraded inside PLA composites, whether it is combined with CC filler or not. Compared to raw KL, the half-time degradation was 20 days shorter in KL containing composites (**Table 5a**). In this present study, KL content did not impact the corresponding kinetics, since similar biodegradation curves were obtained for PLA/KL-10, PLA/KL-20, PLA/KL-15/CC-5, and PLA/KL-2.5/CC-19 (**Figure 6b**). In addition, the extrusion and injection moulding processes could have partially modified KL carbon structure, allowing then a better accessibility of microorganisms for the biodegradation of composites. As for PLA/lignin composites, few studies reported the effect of lignocellulosic fibres on PLA composites biodegradation rate. Pradhan et al. (2010) studied biodegradation kinetic under simulated aerobic compost (ASTM D5338) of PLA-wheat straw and PLA-soy straw composites. After around 40 days, biodegradation of composites slowed down compared to the raw lignocellulosic fibres. After 70 days, 90% biodegradation was achieved for PLA composites whereas lignocellulosic fibres were 100% degraded around 55 days. Petinakis et al. (2010) studied the degradation of PLA-wood flour composites under aerobic composting conditions (AS ISO 14855) and showed that these composites achieved 60% biodegradation after 80 days, with the same rate as pure PLA. Nowadays, it is stated that the contribution of abiotic hydrolysis in PLA degradation mechanism is of major importance in thermophilic composting medium (Karamanlioglu et al., 2017). High humidity and a temperature above glass transition can favour cleavage of the ester bonds in combination with the action of degrading enzyme released by microorganisms leading to the reduction of PLA molecular weight in acid lactic oligomers and consequently the better biodegradation of PLA could be observed (Agarwal et al., 1998; Husárová et al., 2014). The amorphous PLA matrix used in this study degraded easily in compost medium which is consistent to the fact that generally crystalline regions of PLA are more resistant to decomposition than amorphous regions (Husárová et al., 2014; Tokiwa and Calabia, 2006). Nevertheless, the PLA/CC-10 composite could not be fully mineralized by microorganisms since 80% biodegradation plateau was reached after 63 days (**Figure 6c**). On the contrary, when KL was part of the composite, such combination favoured composites biodegradation. Since KL is a rather alkaline compound, a pH variation might

occur inside compost in presence of KL. It is known that PLA degradation rate increases in alkaline media because hydroxide ions can catalyse ester bonds cleavage (Cam et al., 1995; Tsuji and Ikada, 1998), supporting our observations. Finally, we titrated an extra decomposition of the organic carbon from the compost in the reactors containing test materials (except for KL and PLA/CC-10). The phenomena, called «priming effect», has frequently been reported in composting medium containing lignocellulosic materials (Bingeman et al., 1953 ; Kuzyakov et al., 2000). This extra mineralization arises by means of co-metabolism after addition of an easily degradable substrate to the soil (Kuzyakov et al., 2000).

4. Conclusions

This study investigated for the first time an upgrading route for corn cob (CC) and Kraft lignin (KL) into polymeric materials. These by-products from forest and agriculture industries could partially replace PLA to offer 100% plant-based and biodegradable biocomposites. The main objective was to support circular economy by exploring new biocomposite formulations, and potentially replace a part of the PLA matrix to decrease the global cost of the agromaterial. Both fillers were thermally stable at 200°C, allowing their use for industrial scale up extrusion and injection moulding processing methods. As observed, the overall thermal stability of the biocomposites was negatively impacted by filler addition. Nevertheless, both CC and KL acted as nucleating agents and favoured cold crystallization of PLA during processes. Addition of consequent amount of KL, *i.e* 20 wt%, led to an interesting observed decrease of PLA glass transition temperature and a notable loss of material flexural strength properties. According to FT-IR analysis, matrix hydrolysis and/or PLA-KL coupling may have also happened during processing. By combining CC (9 wt%) and KL (2.5 wt%), the obtained lignocellulose-based composites exhibited a flexural strength of 84 MPa which is closed to mechanical properties of pure PLA-A proper wetting of PLA onto CC particles demonstrated a good compatibility at matrix/fibre interface. Surface energy of biocomposites was calculated and contact angle of water showed their hydrophilic behaviour CC filler entirely degraded according to a double sigmoid kinetic model whereas KL exhibited maximum 64% degradation. Surprisingly, biocomposites containing KL were entirely mineralized within 2 months of industrial composting whereas PLA/CC composite reached a plateau at 80% mineralization.

In perspective, the use of chemical coupling agents or enzymes such as laccases from *Trametes Versicolor* could be investigated to accomplish fibre-polymers coupling and improve mechanical properties of these novel biocomposites.

Author Contributions: Conceptualization, A.T. and L.M.; methodology, A.T., B.N. and L.M.; software, B.N.; validation, F.A., H.de.B. and E.G.; formal analysis, A.T., B.N., F.A., E.B., H.de.B. and G.C.; investigation, A.T., B.N., E.G. and L.M.; resources, F.A., E.B., G.C., L.M, and P.M.; writing—original draft preparation, A.T.; writing—review and editing, A.T., B.N., F.A., H.de.B., G.C., E.G., L.M., P.M. and C.D.; supervision, H.de.B., P.M. and C.D.; project administration, H.de.B., C.-G.D., P.M. and C.D; funding acquisition, C.-G.D. and P.M. All authors have read and agreed to the published version of the manuscript.

Funding: This research was funded by the Région Auvergne-Rhône-Alpes and the European Regional Development Fund.

Acknowledgments: Authors acknowledge the French cluster Vegepolys Valley and Limagrain for supplying corn cobs, FPinnovations for supplying Kraft lignin, Valagro Carbone Renouvelable company for running extrusion trials, and the Lycée Germaine Tillion (Raphaël Dalbera and the students Corentin Chombeau, Romain Gerenton, Thibault Rodrigues, and Clément Pichot) for their technical support in injection-moulding.

Data Availability Statement: The data presented in this study are available on request from the corresponding author.

Conflicts of Interest: The authors declare no conflict of interest.

References

Agarwal, M., Koelling, K.W., Chalmers, J.J., 1998. Characterization of the degradation of polylactic acid polymer in a solid substrate environment. Biotechnol. Prog. 14, 517–526. https://doi.org/10.1021/bp980015p

Agustin-Salazar S., Cerruti P., Medina-Juárez L.-A., Scarinzi G., Malinconico M., Soto-Valdez H., Gamez-Meza,H.,2018, Lignin and holocellulose from pecan nutshell as reinforcing fillers in poly (lactic acid) biocomposites, Int.J. Biol.Macromol., 115, 727-736,https://doi.org/10.1016/j.ijbiomac.2018.04.120.

Anwer, M.A.S., Naguib, H.E., Celzard, A., Fierro, V., 2015. Comparison of the thermal, dynamic mechanical and morphological properties of PLA-Lignin & PLA-Tannin particulate green composites. Compos. Part B Eng. 82, 92–99. https://doi.org/10.1016/j.compositesb.2015.08.028

Azwa, Z.N., Yousif, B.F., Manalo, A.C., Karunasena, W., 2013. A review on the degradability of polymeric composites based on natural fibres. Mater. Des. https://doi.org/10.1016/j.matdes.2012.11.025

Berlin, A., Balakshin, M., 2014. Industrial Lignins: Analysis, Properties, and Applications, in: Bioenergy Research: Advances and Applications. Elsevier Inc., pp. 315–336. https://doi.org/10.1016/B978-0-444-59561-4.00018-8

Bingeman, C.W., Varner, J.E., Martin, W.P., 1953. The Effect of the Addition of Organic Materials on the Decomposition of an Organic Soil. Soil Sci. Soc. Am. J. 17, 34–38. https://doi.org/10.2136/sssaj1953.03615995001700010008x

Bužarovska, A., Blazevska-Gilev, J., Pérez-Martnez, B.T., Balahura, L.R., Pircalabioru, G.G., Dinescu, S., Costache, M., 2021. Poly(l-lactic acid)/alkali lignin composites: properties, biocompatibility, cytotoxicity and antimicrobial behavior. J. Mater. Sci. 56, 13785–13800. https://doi.org/10.1007/s10853-021-06185-6

Calmon, A., Silvestre, F., Bellon Maurel, V., Feuilloley, P., 2000. Modèle de prédiction de la dégradation des matériaux polymères en milieu réel. Ingénieries eau-agriculture-territoires, Lavoisier 21, 41–49.

Cam, D., Hyon, S. hyu, Ikada, Y., 1995. Degradation of high molecular weight poly(l-lactide) in alkaline medium. Biomaterials 16, 833–843. https://doi.org/10.1016/0142-9612(95)94144-A

Chevillard, A., Angellier-Coussy, H., Cuq, B., Guillard, V., César, G., Gontard, N., Gastaldi, E., 2011. How the biodegradability of wheat gluten-based agromaterial can be modulated by adding nanoclays. Polym. Degrad. Stab. 96, 2088–2097. https://doi.org/10.1016/j.polymdegradstab.2011.09.024

Chun, K.S., Husseinsyah, S., 2014. Polylactic acid/corn cob eco-composites. J. Thermoplast. Compos. Mater. 27, 1667–1678. https://doi.org/10.1177/0892705712475008

David, G., Michel, J., Gastaldi, E., Gontard, N., Angellier-Coussy, H., 2019. How Vine Shoots as Fillers Impact the Biodegradation of PHBV-Based Composites. Int. J. Mol. Sci. 21, 228. https://doi.org/10.3390/ijms21010228

Décriaud-Calmon, A., 1998. Évaluation objective de la biodégradabilité des matériaux polymères : mise au point d'une méthode et d'un dispositif instrumental. INPT.

Dessbesell, L., Paleologou, M., Leitch, M., Pulkki, R., Xu, C. (Charles), 2020. Global lignin supply overview and kraft lignin potential as an alternative for petroleum-based polymers. Renew. Sustain. Energy Rev. https://doi.org/10.1016/j.rser.2020.109768

Faludi, G., Dora, G., Renner, K., Móczó, J., Pukánszky, B., 2013. Biocomposite from polylactic acid and lignocellulosic fibers: Structure-property correlations. Carbohydr. Polym. 92, 1767–1775. https://doi.org/10.1016/j.carbpol.2012.11.006

Faruk, O., Sain, M., 2015. Lignin in Polymer Composites, Lignin in Polymer Composites. Elsevier Inc. https://doi.org/10.1016/C2014-0-01101-X

Gao, H., Qiang, T., 2017. Fracture Surface Morphology and Impact Strength of Cellulose/PLA Composites. Materials (Basel). 10, 624. https://doi.org/10.3390/ma10060624

Gkartzou, E., Koumoulos, E.P., Charitidis, C.A., 2017. Production and 3D printing processing of bio-based

thermoplastic filament. Manuf. Rev. 4, 1. https://doi.org/10.1051/mfreview/2016020

Gordobil, O., Delucis, R., Egüés, I., Labidi, J., 2015. Kraft lignin as filler in PLA to improve ductility and thermal properties. Ind. Crops Prod. 72, 46–53. https://doi.org/10.1016/j.indcrop.2015.01.055

Gordobil, O., Egüés, I., Llano-Ponte, R., Labidi, J., 2014. Physicochemical properties of PLA lignin blends. Polym. Degrad. Stab. 108, 330–338. https://doi.org/10.1016/j.polymdegradstab.2014.01.002

Gordobil, O., Moriana, R., Zhang, L., Labidi, J., Sevastyanova, O., 2016. Assesment of technical lignins for uses in biofuels and biomaterials: Structure-related properties, proximate analysis and chemical modification. Ind. Crops Prod. 83, 155–165. https://doi.org/10.1016/j.indcrop.2015.12.048

Goriparthi, B.K., Suman, K.N.S., Mohan Rao, N., 2012. Effect of fiber surface treatments on mechanical and abrasive wear performance of polylactide/jute composites, in: Composites Part A: Applied Science and Manufacturing. Elsevier, pp. 1800–1808. https://doi.org/10.1016/j.compositesa.2012.05.007

Gorrasi, G., Pantani, R., 2013. Effect of PLA grades and morphologies on hydrolytic degradation at composting temperature: Assessment of structural modification and kinetic parameters. Polym. Degrad. Stab. 98, 1006–1014. https://doi.org/10.1016/j.polymdegradstab.2013.02.005

Guo, H., He, M., Huang, R., Qi, W., Guo, W., Su, R., He, Z., 2014. Changes in the supramolecular structures of cellulose after hydrolysis studied by terahertz spectroscopy and other methods. RSC Adv. 4, 57945–57952. https://doi.org/10.1039/c4ra08314h

Husárová, L., Pekařová, S., Stloukal, P., Kucharzcyk, P., Verney, V., Commereuc, S., Ramone, A., Koutny, M., 2014. Identification of important abiotic and biotic factors in the biodegradation of poly(l-lactic acid). Int. J. Biol. Macromol. 71, 155–162. https://doi.org/10.1016/j.ijbiomac.2014.04.050

Karamanlioglu, M., Preziosi, R., Robson, G.D., 2017. Abiotic and biotic environmental degradation of the bioplastic polymer poly(lactic acid): A review. Polym. Degrad. Stab. https://doi.org/10.1016/j.polymdegradstab.2017.01.009

Komal, U.K., Lila, M.K., Singh, I., 2020. PLA/banana fiber based sustainable biocomposites: A manufacturing perspective. Compos. Part B Eng. 180, 107535. https://doi.org/10.1016/j.compositesb.2019.107535

Kumar, A., Tumu, V.R., 2019. Physicochemical properties of the electron beam irradiated bamboo powder and its bio-composites with PLA. Compos. Part B Eng. 175, 107098. https://doi.org/10.1016/j.compositesb.2019.107098

Kumar, A., Tumu, V.R., Ray Chowdhury, S., Ramana, R.R., 2019. A green physical approach to compatibilize a bio-based poly (lactic acid)/lignin blend for better mechanical, thermal and degradation properties. Int. J. Biol. Macromol. 121, 588–600. https://doi.org/10.1016/j.ijbiomac.2018.10.057

Kumar, S., Negi, Y.S., Upadhyaya, J.S., 2010. Studies on characterization of corn cob based nanoparticles. Adv. Mater. Lett. 1, 246–253. https://doi.org/10.5185/amlett.2010.9164

Kuzyakov, Y., Friedel, J.K., Stahr, K., 2000. Review of mechanisms and quantification of priming effects. Soil Biol. Biochem. https://doi.org/10.1016/S0038-0717(00)00084-5

Lezak E., Kulinski Z., Masirek R., Piorkowska E., Pracella M., Gadzinowska K., 2008, Mechnaical and thermal properties of green polylactide composites with natural fillers, Macromol. Biosci. 8, 1190-1200, https://doi.org/10.1002/mabi.200800040

Li, M., Cheng, Y.L., Fu, N., Li, D., Adhikari, B., Chen, X.D., 2014. Isolation and characterization of corncob

cellulose fibers using microwave-assisted chemical treatments. Int. J. Food Eng. 10, 427–436. https://doi.org/10.1515/ijfe-2014-0052

Lila, M.K., Shukla, K., Komal, U.K., Singh, I., 2019. Accelerated thermal ageing behaviour of bagasse fibers reinforced Poly (Lactic Acid) based biocomposites. Compos. Part B Eng. 156, 121–127. https://doi.org/10.1016/j.compositesb.2018.08.068

Luo, H., Xiong, G., Ma, C., Chang, P., Yao, F., Zhu, Y., Zhang, C., Wan, Y., 2014. Mechanical and thermo-mechanical behaviors of sizing-treated corn fiber/polylactide composites. Polym. Test. 39, 45–52. https://doi.org/10.1016/j.polymertesting.2014.07.014

Mansor, M.R., Salit, M.S., Zainudin, E.S., Aziz, N.A., Ariff, H., 2015. Life cycle assessment of natural fiber polymer composites, Agricultural Biomass Based Potential Materials. Springer International Publishing. https://doi.org/10.1007/978-3-319-13847-3_6

Miller, J., Faleiros, M., Pilla, L., Bodart, A.-C., 2016. Lignin: Technology, Applications, and Markets.

Mimini, V., Sykacek, E., Hashim, S.N.A., Holzweber, J., Hettegger, H., Fackler, K., Potthast, A., Mundigler, N., Rosenau, T., 2019. Compatibility of Kraft Lignin, Organosolv Lignin and Lignosulfonate With PLA in 3D Printing. J. Wood Chem. Technol. 39, 14–30. https://doi.org/10.1080/02773813.2018.1488875

Misra, M., Pandey, J.K., Mohanty, A.K., 2015. Biocomposites: Design and Mechanical Performance, Biocomposites: Design and Mechanical Performance. Elsevier Inc. https://doi.org/10.1016/C2014-0-02693-7

Musioł, M., Sikorska, W., Adamus, G., Janeczek, H., Richert, J., Malinowski, R., Jiang, G., Kowalczuk, M., 2016. Forensic engineering of advanced polymeric materials. Part III - Biodegradation of thermoformed rigid PLA packaging under industrial composting conditions. Waste Manag. 52, 69–76. https://doi.org/10.1016/j.wasman.2016.04.016

Nilsson, T., 2009. Biological wood degradation, in: Wood Chemistry and Wood Biotechnology. Walter de Gruyter GmbH and Co. KG, pp. 219–244. https://doi.org/10.1515/9783110213409.219

Ogah, A.O., Afiukwa, J.N., 2014. Characterization and comparison of mechanical behavior of agro fiber-filled high-density polyethylene bio-composites. J. Reinf. Plast. Compos. 33, 37–46. https://doi.org/10.1177/0731684413509425

Onuoha, C., Onyemaobi, O., Anyakwo, C., Onuegbu, G., 2017. Morphology and Physical/End-Use Properties of Recycled Polypropylene-Corn Cob Powder Composites. Int. J. Eng. Technol. 11, 1–12. https://doi.org/10.18052/www.scipress.com/ijet.11.1

Owens, D.K., Wendt, R.C., 1969. Estimation of the surface free energy of polymers. J. Appl. Polym. Sci. 13, 1741–1747. https://doi.org/10.1002/app.1969.070130815

Panthapulakkal, S., Sain, M., 2007. Agro-residue reinforced high-density polyethylene composites: Fiber characterization and analysis of composite properties. Compos. Part A Appl. Sci. Manuf. 38, 1445–1454. https://doi.org/10.1016/j.compositesa.2007.01.015

Petinakis, E., Liu, X., Yu, L., Way, C., Sangwan, P., Dean, K., Bateman, S., Edward, G., 2010. Biodegradation and thermal decomposition of poly(lactic acid)-based materials reinforced by hydrophilic fillers. Polym. Degrad. Stab. 95, 1704–1707. https://doi.org/10.1016/j.polymdegradstab.2010.05.027

Poletto, M., 2018. Lignin - Trends and Applications, Lignin - Trends and Applications. InTech. https://doi.org/10.5772/intechopen.68464

Pradhan, R., Misra, M., Erickson, L., Mohanty, A., 2010. Compostability and biodegradation study of PLA-wheat straw and PLA-soy straw based green composites in simulated composting bioreactor. Bioresour. Technol. 101, 8489–8491. https://doi.org/10.1016/j.biortech.2010.06.053

Rajeshkumar, G., Arvindh Seshadri, S., Devnani, G.L., Sanjay, M.R., Siengchin, S., Prakash Maran, J., Al-Dhabi, N.A., Karuppiah, P., Mariadhas, V.A., Sivarajasekar, N., Ronaldo Anuf, A., 2021. Environment friendly, renewable and sustainable poly lactic acid (PLA) based natural fiber reinforced composites – A comprehensive review. J. Clean. Prod. 310, 127483. https://doi.org/10.1016/j.jclepro.2021.127483

Ravi Theja Reddy S., Ratna Prasad A.V., Ramanaiah K., 2021, Tensile and flexural properties of biodegradable jute fiber reinforced poly lactic acid composites,Materials Today: Proceedings, 44, 917-921, https://doi.org/10.1016/j.matpr.2020.10.806.

Schwietzke, S., Kim, Y., Ximenes, E., Mosier, N., Ladisch, M., 2009. Ethanol production from maize, in: Biotechnology in Agriculture and Forestry. Springer International Publishing, pp. 347–364. https://doi.org/10.1007/978-3-540-68922-5_23

Siakeng, R., Jawaid, M., Ariffin, H., Sapuan, S.M., Asim, M., Saba, N., 2019. Natural fiber reinforced polylactic acid composites: A review. Polym. Compos. 40, 446–463. https://doi.org/10.1002/pc.24747

Silva, T.F. da, Menezes, F., Montagna, L.S., Lemes, A.P., Passador, F.R., 2019. Effect of lignin as accelerator of the biodegradation process of poly(lactic acid)/lignin composites. Mater. Sci. Eng. B Solid-State Mater. Adv. Technol. 251, 114441. https://doi.org/10.1016/j.mseb.2019.114441

Sin, L.T., Tueen, B.S., 2019. Environmental Assessment of Poly(Lactic Acid) and International Standards, in: Polylactic Acid. Elsevier, pp. 365–387. https://doi.org/10.1016/b978-0-12-814472-5.00012-1

Skoczinski, P., Carus, M., de Guzman, D., Käb, H., Chinthapalli, R., Ravenstijn, J., Baltus, W., Raschka, A., 2021. Bio-based Building Blocks and Polymers – Global Capacities, Production and Trends 2020 – 2025.

Spiridon, I., Leluk, K., Resmerita, A.M., Darie, R.N., 2015. Evaluation of PLA-lignin bioplastics properties before and after accelerated weathering. Compos. Part B Eng. 69, 342–349. https://doi.org/10.1016/j.compositesb.2014.10.006

Stark, N.M., Gardner, D.J., 2008. Outdoor durability of wood-polymer composites, in: Wood-Polymer Composites. Elsevier Ltd., pp. 142–165. https://doi.org/10.1533/9781845694579.142

Tan, Y., Zhang, X., Qu, J.P., 2019. Preparation and characterization of poly(lactic acid)/sisal fiber bio-composites under continuous elongation flow. J. Polym. Eng. 39, 76–84. https://doi.org/10.1515/polyeng-2018-0075

Tanase-Opedal, M., Espinosa, E., Rodríguez, A., Chinga-Carrasco, G., 2019. Lignin: A Biopolymer from Forestry Biomass for Biocomposites and 3D Printing. Materials (Basel). 12, 3006. https://doi.org/10.3390/ma12183006

Tokiwa Y, Calabia BP. Biodegradability and biodegradation of poly(lactide). Appl Microbiol Biotechnol 2006;72:244–51. https://doi.org/10.1007/s00253-006-0488-1.

Tribot, A., Delattre, C., Badel, E., Dussap, C.-G., Michaud, P., de Baynast, H., 2018. Design of experiments for bio-based composites with lignosulfonates matrix and corn cob fibers. Ind. Crops Prod. 123.

https://doi.org/10.1016/j.indcrop.2018.07.019

Tribot, Amélie, Delattre, C., Badel, E., Dussap, C.G., Michaud, P., de Baynast, H., 2018. Design of experiments for bio-based composites with lignosulfonates matrix and corn cob fibers. Ind. Crops Prod. 123, 539–545. https://doi.org/10.1016/j.indcrop.2018.07.019

Tsuji, H., Ikada, Y., 1998. Properties and morphology of poly(L-lactide). II. Hydrolysis in alkaline solution. J. Polym. Sci. Part A Polym. Chem. 36, 59–66. https://doi.org/10.1002/(SICI)1099-0518(19980115)36:1<59::AID-POLA9>3.0.CO;2-X

Tuomela, M., Vikman, M., Hatakka, A., Itävaara, M., 2000. Biodegradation of lignin in a compost environment: A review. Bioresour. Technol. 72, 169–183. https://doi.org/10.1016/S0960-8524(99)00104-2

Wang, N., Zhang, C., Zhu, W., Weng, Y., 2020. Improving Interfacial Adhesion of PLA/Lignin Composites by One-Step Solvent-Free Modification Method, 8,1139-1149. https://doi.org/10.32604/jrm.2020.09961

Wan, Y., Wu, H., Huang, L., Zhang, J., Tan, S., Cai, X., 2018. Preparation and characterization of corn cob/polypropylene composite reinforced by wood ash. Polym. Bull. 75, 2125–2138. https://doi.org/10.1007/s00289-017-2149-1

Wang, X., Jia, Y., Liu, Z., Miao, J., 2018. Influence of the Lignin Content on the Properties of Poly(Lactic Acid)/lignin-Containing Cellulose Nanofibrils Composite Films. Polymers (Basel). 10, 1013. https://doi.org/10.3390/polym10091013

Graphical abstract:

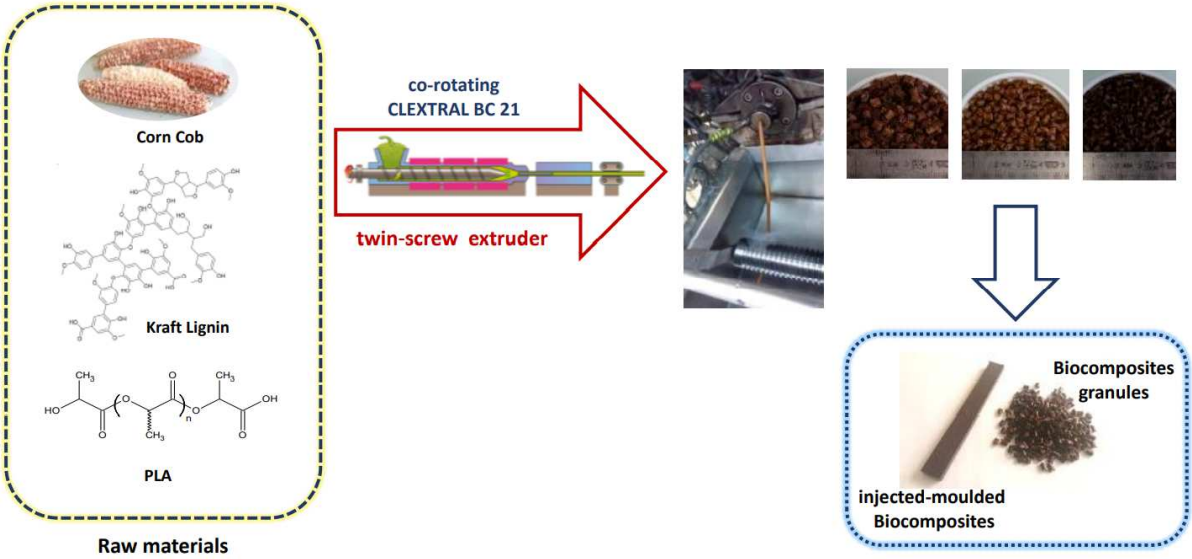
Corn Cob
Kraft Lignin
PLA
Raw materials
co-rotating
CLEXTRAL BC 21
twin-screw extruder
Biocomposites
granules
injected-moulded
Biocomposites

Table 1. Parameters during the twin-screw extrusion process. 718

Recipes	Material 1; Material 2	Feeding of materials 1; and 2 (kg/h)	Temperatures from feed to nose (°C)	Screw speeds (rpm)	Pressures (10^5 Pa)	% of maximum torque
1	PLA; CC	9; 1	20/110/5x190/2x185	260	60	68
2	PLA; CC	7.5; 2.5	20/110/5x190/2x185	260	60	68
3	PLA; Kraft lignin	9; 1	20/110/5x190/2x185	449	60	56
4	PLA ; Kraft lignin	6.4; 1.6	20/110/5x190/2x185	418	47	54
5	PLA; Kraft lignin	5.6; 2.4	15/75/160/4x190/2x185	302	58	60

719

720

Table 2. Composition of the injected samples and their injection temperatures

Samples	wt% (Recipe Table 1)	PLA (wt%)	KL (wt%)	CC (wt%)	Injection temperatures (°C)
PLA	-	100.00	-	-	125 – 170
PLA/KL-10	100% (3)	90.00	10.00	-	125 – 165
PLA/KL-20	100% (4)	80.00	20.00	-	125 – 165
PLA/CC-10	100% (1)	90.00	-	10.00	125 – 165
PLA/KL-2.5/CC-9	87.5% (1): 12.5% (4)	88.75	2.50	8.75	110 – 150
PLA/KL-5/CC-12.5	50% (2): 50% (3)	82.50	5.00	12.50	105 – 145
PLA/KL-2.5/CC-19	75% (2): 25% (3)	82.50	2.50	18.75	105 – 145
PLA/KL-15/CC-5	50% (1): 50% (5)	80.00	15.00	5.00	125 – 165

Table 3. Differential Scanning Calorimetry results: glass transition temperatures (Tg), cold crystallization temperatures and enthalpies (Tcc and ΔHcc), melting temperatures and enthalpies (Tm and ΔHm), % of crystallinity (Xc) of raw materials and composites.

Samples	**Tg (°C)**	**Tcc (°C)**	**ΔHcc (J g^{-1})**	**Tm (°C)**	**ΔHm (J g^{-1})**	**Xc (%)**
PLA	60.5	123.7	5.3	152.1	6.0	10.8
PLA/KL-10	61.3	124.5	20.1	150.8	20.1	0.0
PLA/KL-20	56.4	121.5	24.3	146.5	24.1	0.0
PLA/CC-10	60.9	118.0	21.9	149.5	22.7	3.6
PLA/KL-2.5/CC-9	58.3	117.3	26.5	149.2	28.0	5.3
PLA/KL-5/CC-12.5	58.1	120.6	31.1	148.7	30.5	0.0
PLA/KL-2.5/CC-19	58.4	119.9	9.6	148.0	10.2	5.4
PLA/KL-15/CC-5	55.9	123.3	9.1	148.7	9.8	7.3

Table 4. Surface energy of solid composites and PLA (σs^{Total}), polar component (σs^{Polar}), and dispersive component ($\sigma s^{Dispersive}$) of their surface energy and contact angle of the different solvents on polymer/composites surfaces.

Samples	σ_s^{Total} **(mN/m)**	σ_s^{Polar} **(mN/m)**	$\sigma_s^{Dispersive}$ **(mN/m)**	$\sigma_s^{Polar}/\sigma_s^{Dispersive}$	θ_{water} (°)	$\theta_{glycerol}$ (°)	$\theta_{ethylene\ glycol}$ (°)	$\theta_{formamide}$ (°)
PLA	30.6	20.3	10.4	2.0	73.2	69.6	57.8	56.7
PLA/KL-20	27.6	17.8	9.9	1.8	80.5	76.8	57.7	62.5
PLA/CC-10	28.7	20.0	8.7	2.3	76.3	74.1	60.2	59.7
PLA/KL-15/CC-5	27.8	18.7	9.1	2.1	75.8	77.2	62.4	62.4

Table 5. (**a**) Hill parameters (Equation 2) modelling microcellulose biodegradation (i.e. positive control), Kraft lignin (KL), and composites biodegradation; (**b**) Boltzmann parameters (Equation 3) modelling corn cob (CC) biodegradation.

(a)

Samples	**Deg_{max} (%)**	**n (-)**	**k (days)**	**R^2**
microcellulose	118.2	1.446	13.7	0.998
KL	64.1	1.821	56.9	0.988
PLA/CC-10	79.6	4.899	28.0	0.991
PLA/KL-10	120.6	3.135	39.2	0.997
PLA/KL-20	120.4	2.998	39.7	0.996
PLA/KL-15/CC-5	124.1	2.830	38.3	0.995
PLA/KL-2.5/CC-19	121.1	2.551	34.6	0.993

(b)

Sample	**Deg_{max} (%)**	**h_1 (-)**	**h_2 (-)**	**p (-)**	**k_1 (days)**	**k_2 (days)**	**R^2**
CC	109.3	0.330	0.036	0.397	3.1	43.3	0.996

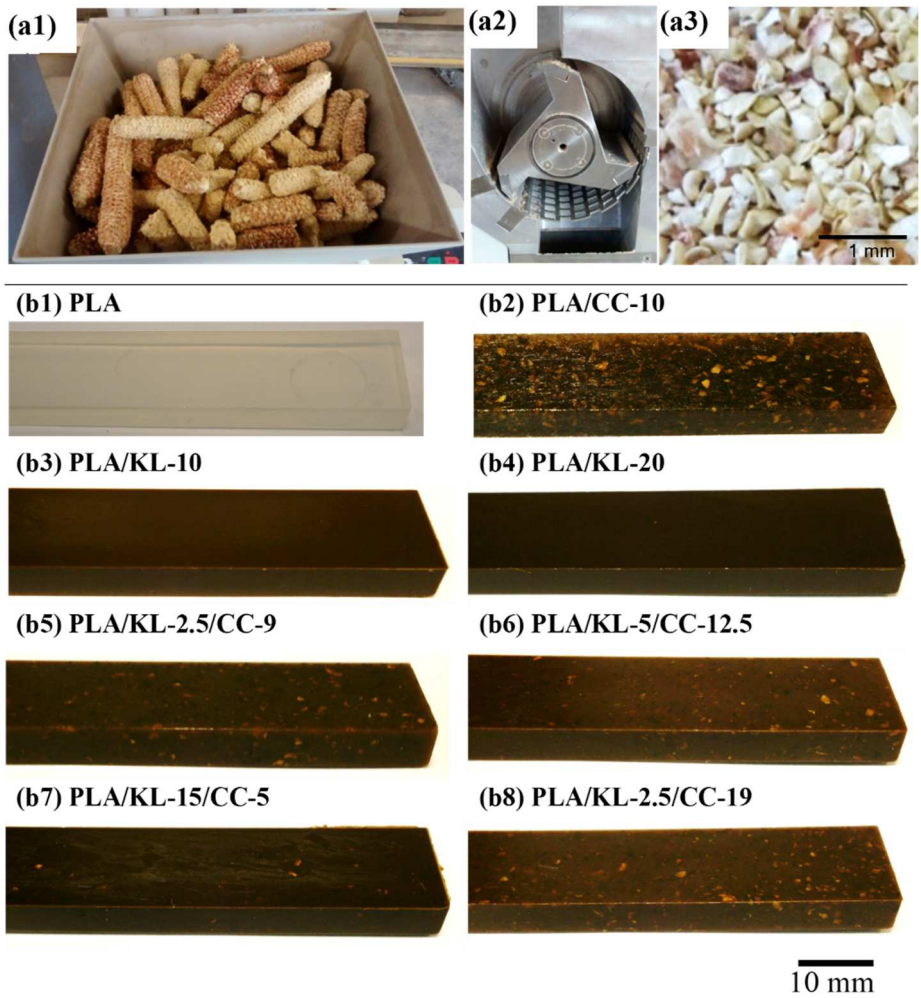

Figure 1. (**a1**) Collected raw and dried corn cobs; (**a2**) Equipment for crushing into particles the raw corn cobs; (**a3**) shattered corn cob fibers (**b1**) Poly(lactic acid) (PLA) test sample after extrusion and injection-moulding; (**b2-b8**) Test samples of composite materials after compounding of PLA, Kraft lignin, and/or corn cob and then injection-moulding.

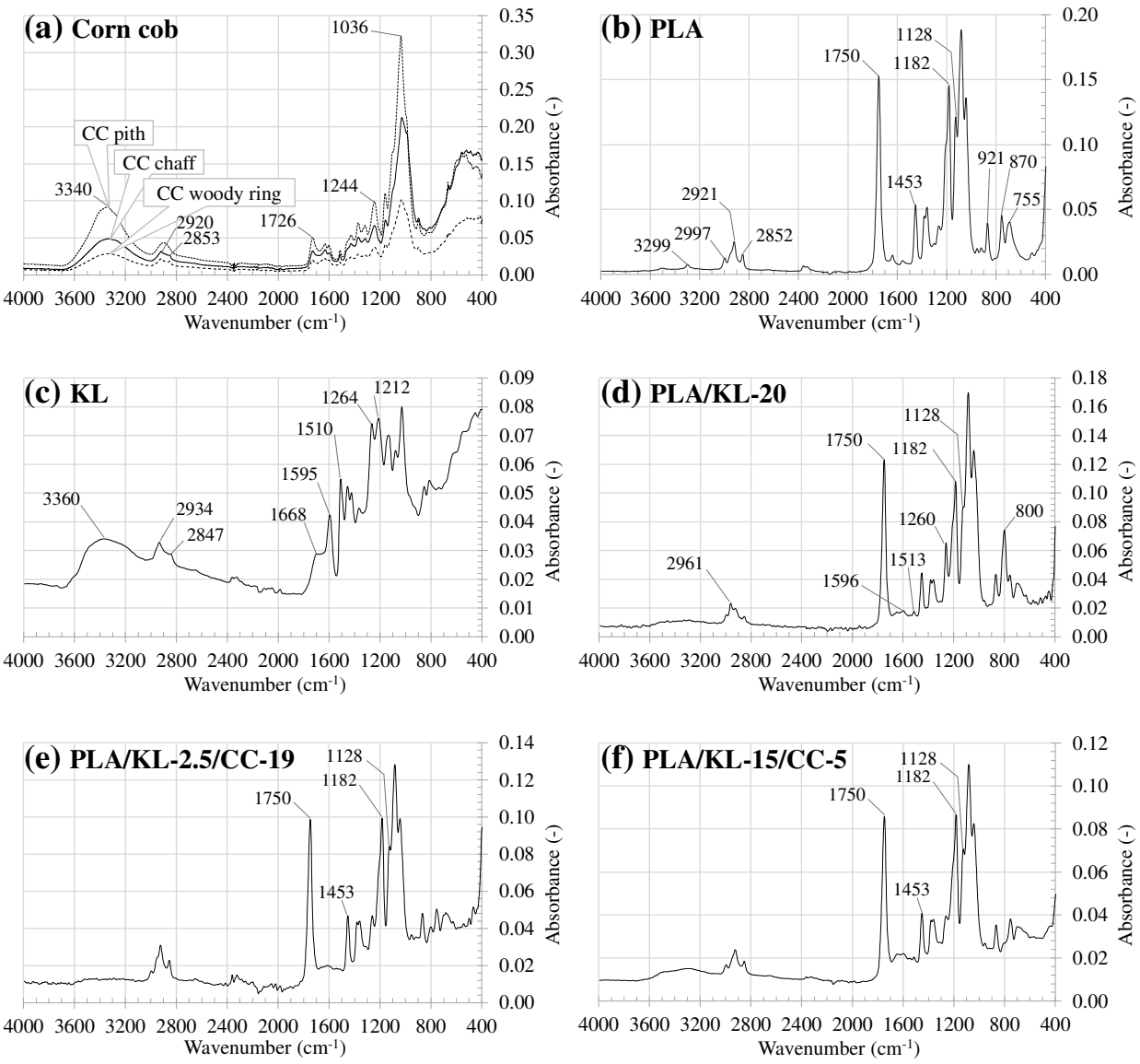

Figure 2. FT-IR spectroscopy of: (**a-c**) raw materials; (**d-f**) composites (with CC = corn cob)

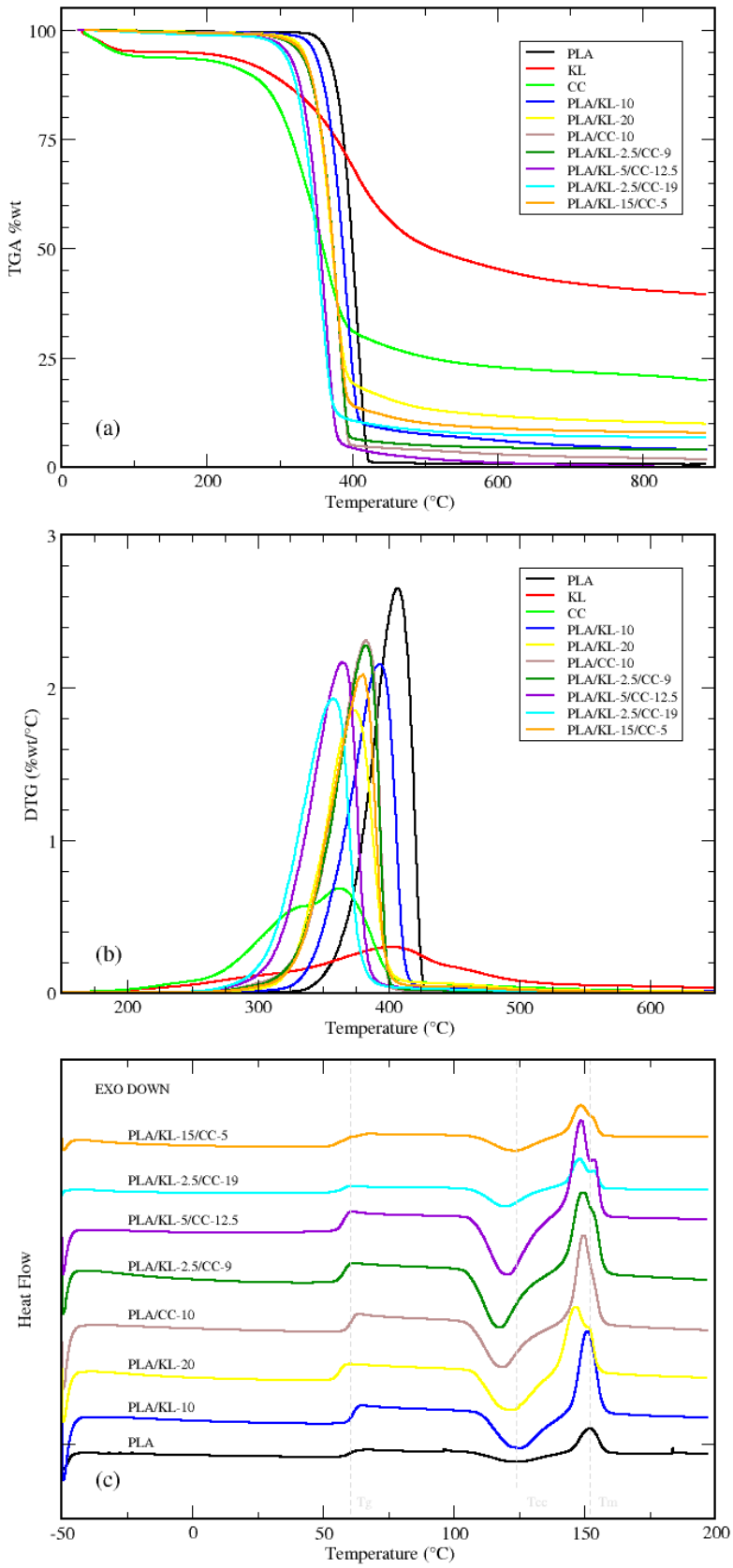

Figure 3. Thermal analyses of PLA, Kraft lignin (KL), corn cob (CC) and their composites: (**a**) Thermogravimetric TG signals; (**b**) Differential thermogravimetric DTG signals; (**c**) Differential Scanning Calorimetry DSC signals during the second heating.

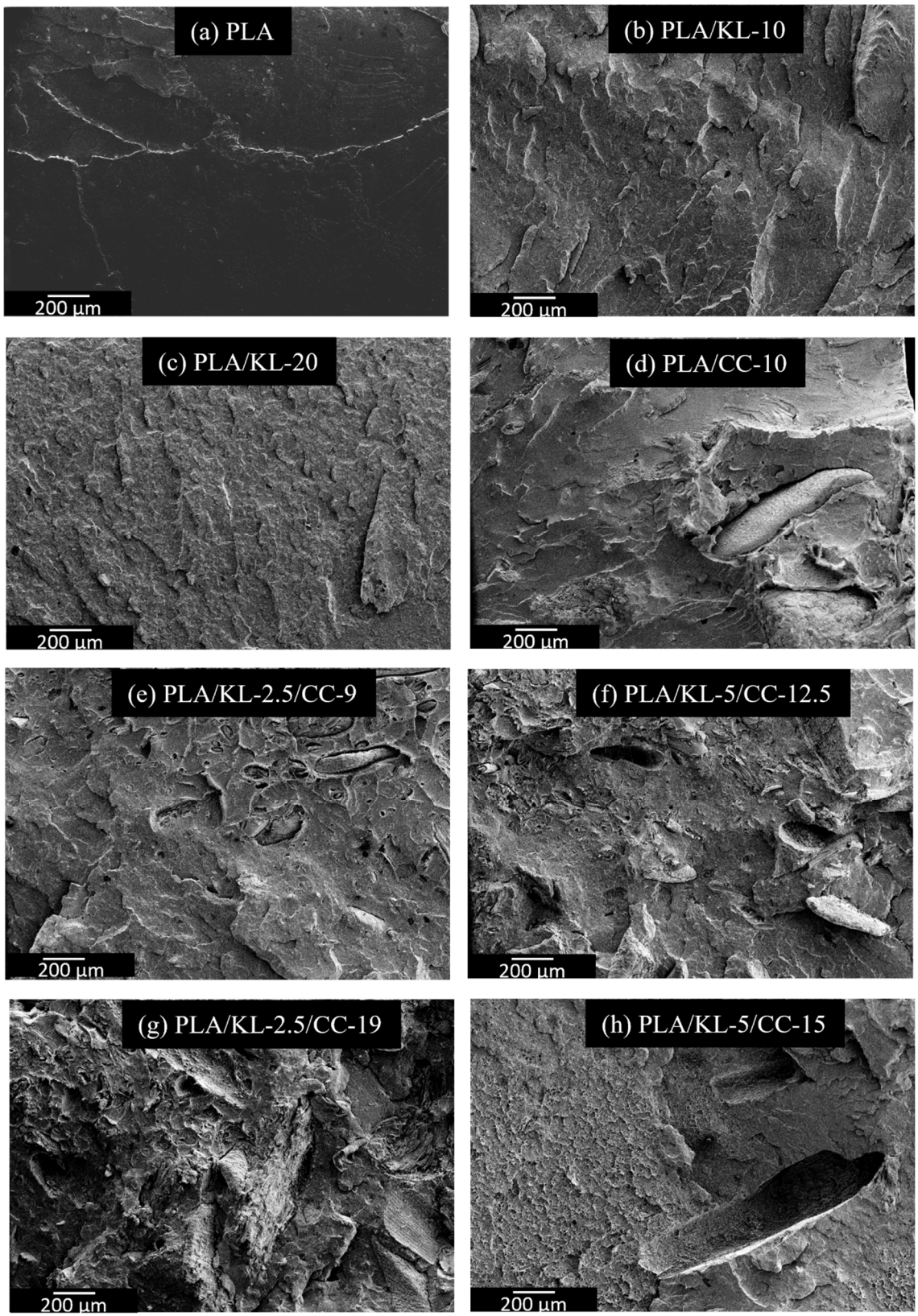

Figure 4. SEM images of PLA and composites test specimens after fracture, containing 2.5 to 20wt% Kraft lignin (KL) and/or 5 to 19wt% corn cob (CC).

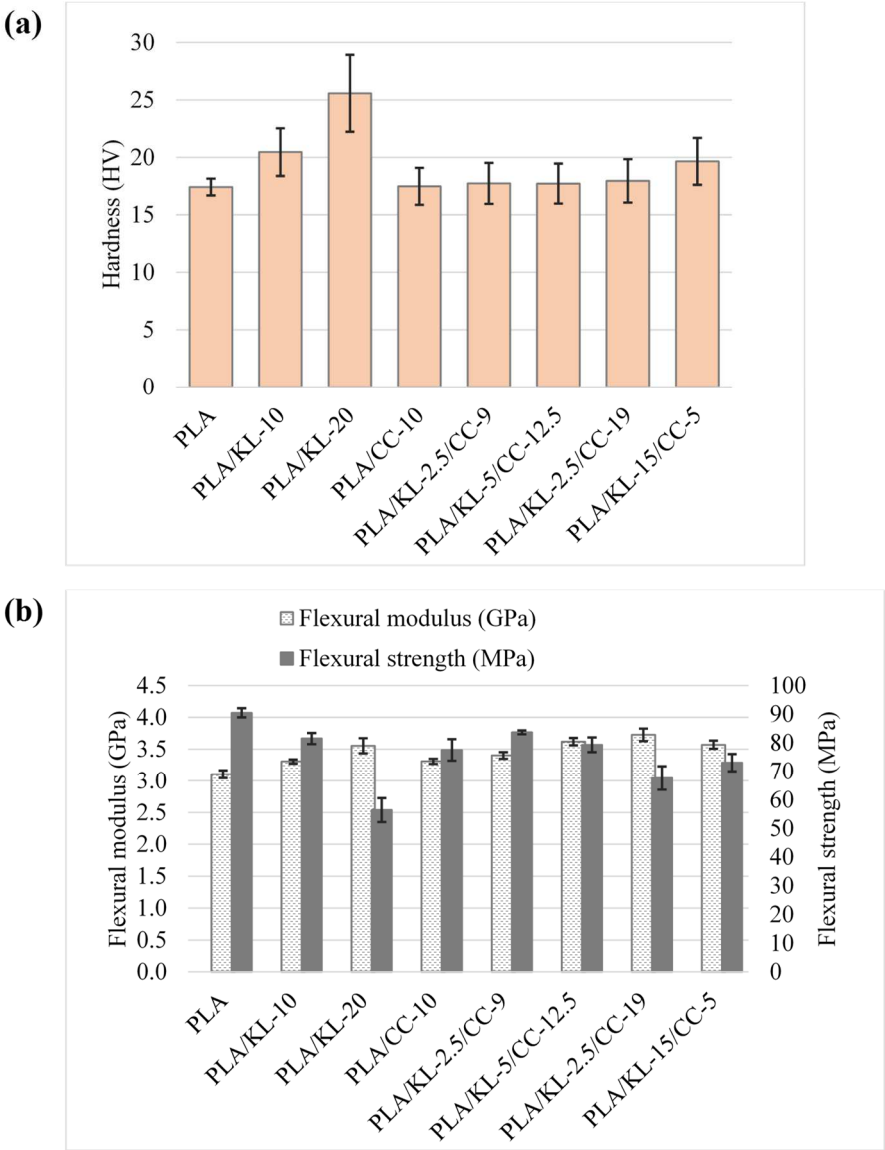

~~**Figure 4**~~ **Figure 5.** Mechanical properties of PLA and composites test specimens containing 2.5 to 20wt% of Kraft lignin and/or 5 to 19wt% of corn cob: (a) Vickers hardness; (b) Flexural modulus and flexural strength at maximum load.

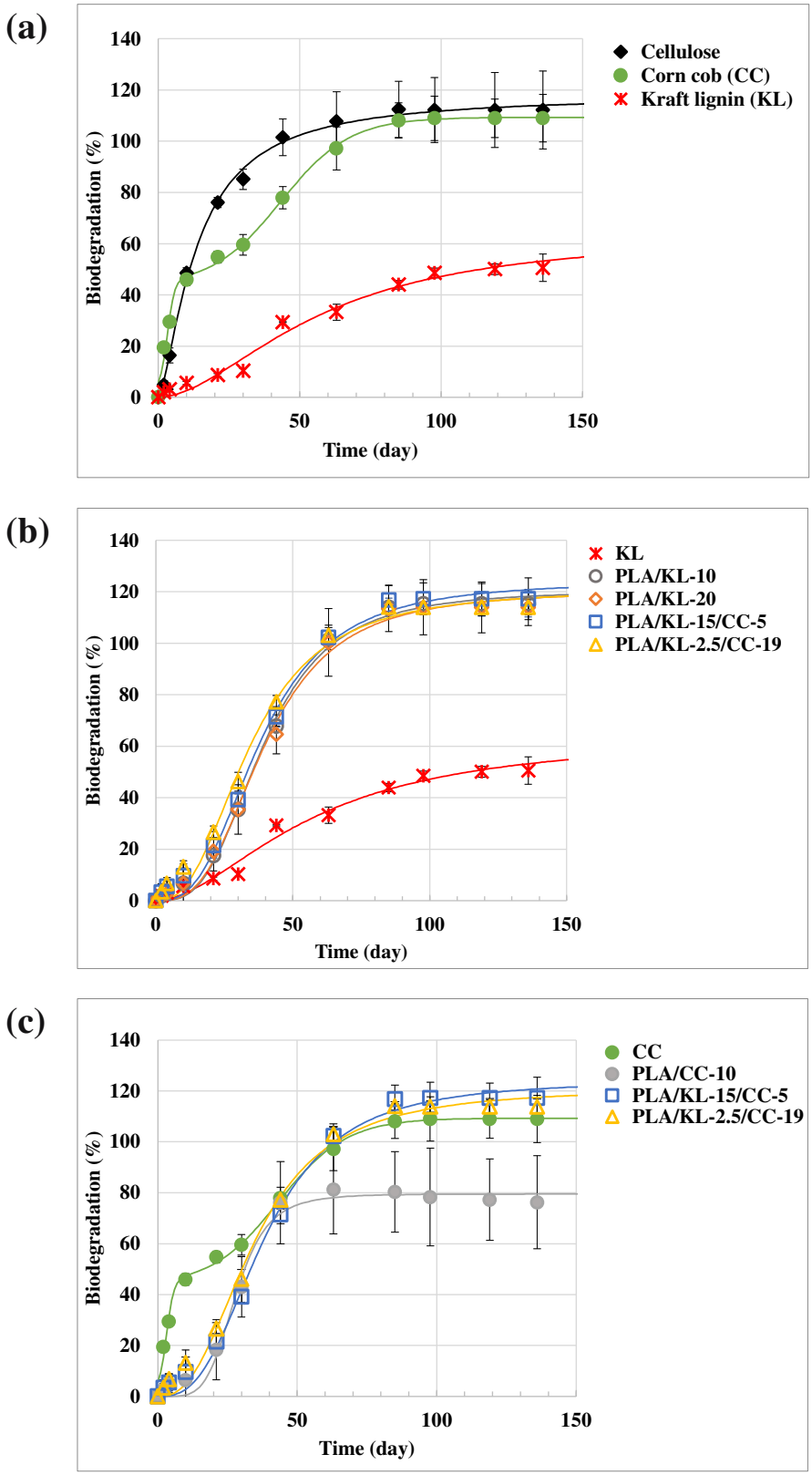

Figure 6. Modelled curves and experimental points of materials biodegradation in industrial composting conditions: (**a**) Positive cellulose control, corn cob particles, and Kraft lignin powder; (**b**) Kraft lignin powder and composites containing Kraft lignin; (**c**) Corn cob particles and composites containing corn cob.

Appendix

Table. Hardness, flexural mechanical properties, and density of injected biocomposites samples

Samples	Vickers hardness (-)	Density (-)	Flexural modulus (GPa)	Flexural strength (MPa)	Flexural deflection (%)
PLA	17.4 ± 0.7	1.215 ± 0.009	3.10 ± 0.06	90.51 ± 1.61	4.01 ± 0.06
PLA/KL-10	20.5 ± 2.1	1.218 ± 0.006	3.31 ± 0.03	81.53 ± 1.90	2.84 ± 0.19
PLA/KL-20	25.6 ± 3.4	1.230 ± 0.007	3.56 ± 0.12	56.39 ± 4.18	1.64 ± 0.14
PLA/CC-10	17.5 ± 1.6	1.244 ± 0.015	3.31 ± 0.04	77.51 ± 3.77	3.31 ± 0.10
PLA/KL-2.5/CC-9	18.0 ± 1.9	1.228 ± 0.011	3.40 ± 0.05	83.67 ± 0.67	3.33 ± 0.06
PLA/KL-2.5/CC-19	17.7 ± 1.8	1.244 ± 0.013	3.73 ± 0.10	67.63 ± 4.17	2.08 ± 0.16
PLA/KL-5/CC-12.5	17.7 ± 1.7	1.249 ± 0.005	3.62 ± 0.06	79.33 ± 2.57	2.67 ± 0.17
PLA/KL-15/CC-5	19.7 ± 2.0	1.251 ± 0.012	3.57 ± 0.06	73.05 ± 3.01	2.28 ± 0.20

Table. TGA of raw materials and composites

Samples	T_{ONSET} (°C)	T_{MIDSET} (°C)	T_{OFFSET} (°C)	Residual weight (%)
PLA	382.1	407.1	419.3	0.6
KL[1]	314.4	402.3	483.7	39.5
CC[1]	297.2	362.3	395.4	19.8
PLA/KL-10	364.6	393.8	408.0	3.9
PLA/KL-20	346.2	374.2	393.4	9.8
~~PLA/KL-30[2]~~	~~348.1~~	~~375.5~~	~~398.1~~	~~11.3~~
PLA/CC-10	353.2	382.7	394.4	1.7
PLA/KL-2.5/CC-9	353.0	383.1	394.3	4.0
PLA/KL-2.5/CC-19	327.1	357.9	373.8	6.7
PLA/KL-5/CC-12.5	334.4	364.7	379.1	4.7
PLA/KL-15/CC-5	350.9	380.6	393.8	7.9

[1]raw material. [2]~~pellet~~